Prediction of the fatigue properties of natural rubber based on the descriptions of the cracks population and of the dissipated energy

Yann Marco, Bertrand Huneau, Isaure Masquelier, V. Le Saux, Pierre Charrier

Test Method

PREDICTION OF FATIGUE PROPERTIES OF NATURAL RUBBER BASED ON THE DESCRIPTIONS OF THE CRACKS POPULATION AND OF THE DISSIPATED ENERGY

Y. Marco[a], B. Huneau[b], I. Masquelier[a], V. Le Saux[a], P. Charrier[c]

[a] ENSTA Bretagne, Institut de Recherche Dupuy de Lôme (IRDL), FRE CNRS 3744, Brest, France
[b] Ecole Centrale de Nantes, Institut de Recherche en Génie Civil et Mécanique (GeM), UMR CNRS 6183, Nantes, France
[c] Vibracoustic, CAE Durability Prediction department, Nantes, France

ABSTRACT

The goal of this paper is to relate the fatigue lifetime to the energy dissipation and the crack population for a Natural Rubber (NR) compound filled with carbon black. First, the dissipated energy is measured by thermal measurements and its evolution with the local strain is described. Then, the crack population under fatigue loading is investigated thanks to interrupted fatigue tests and SEM measurements. The dependency of the evolution of the crack surface density on the local strain and number of cycles is described. Finally, a fatigue criterion is suggested, starting from the basic assumption of accumulation of dissipated energy along the fatigue cycles. Combining the evolution of the dissipated energy and the crack surface density, the energetic criterion can be written as a simple expression using a single parameter. The predictions obtained with the identified criterion are compared with the results from classic fatigue tests and very close agreement is found.

INTRODUCTION

From an industrial point of view, the development of reinforced elastomers resistant to fatigue remains a difficult task because of the complex dissipative behavior exhibited under cyclic loading, and because of the very strong coupling of the failure to the microstructure features, for these heterogeneous materials. As expressed very early [**1-3**], the failure is driven by flaws in the materials, related to geometric singularities or inclusions of different natures [**4-11**]. The understanding of the fatigue behavior and failure should, therefore, require descriptions of both the thermo-mechanical response and the microstructure. To design rubber parts, the literature provides numerous phenomenological criteria to evaluate the fatigue lifetime of elastomeric structures [**12**] and, if some criteria remain fully macroscopic [**13-17**], most of the approaches try to base the macroscopic fatigue criterion on microscopic considerations, both for crack propagation [**18-21**] and initiation approaches [**21-24**]. On the other hand, numerous experimental studies based mostly on optical microscopy [**6, 25**], SEM and X-ray tomography measurements [**5,7-11**], investigated the basic damage mechanisms [**4-11, 25**] and the experimental evolution of the defects initiated under fatigue loading [**25-30**]. Nevertheless, relating the thermo-mechanical response and the failure criteria at the macroscopic scale to the basic fatigue mechanisms around the flaws or cracks remains a difficult challenge because of the numerous factors and scales involved.

A first scale is related to the initial flaw and the understanding of the basic mechanisms involved. For inclusions, three main mechanisms have been identified in the literature (interface failure, break of the inclusion, cavitation between close inclusions [**4, 8, 11, 27, 31**]) but the energy or the mechanical fields needed to initiate a crack are of course dependent on the local configuration and on the nature of both the matrix and filler. Although the nature of the inclusions or cracks, their geometry and the initiation mechanisms can be described and potentially modeled [**32-33**], providing experimental data to assess the energy balance at these scales (typically from 1 to 400 micrometers [**12**]) is clearly more difficult [**10, 34-35**]. The other way round, it is difficult to relate the macroscopic evaluation of the fatigue criteria to these basics mechanisms [**48**] because of the very numerous phenomena involved: viscosity [**36-37**], plasticity [**38**], fatigue damage [**32, 38-39**], crystallization [**40-41**], Mullins effect [**42**], etc.
A second scale deals with the population of the flaws initiated and with the combination of their features (maximum size, size dispersion, spatial dispersion) with the gradients of mechanical fields [**30, 43-44**]. Although this aspect is well integrated by recent modeling approaches [**22, 24, 45-46**], the correlation to real flaws or cracks populations is still to be investigated. Moreover, the design approaches are often based on a critical configuration approach, assuming that one, or a few, defects [**45**] would experience the worst configuration in size, orientation and local mechanical fields [**25**]. For materials exhibiting good resistance to crack propagation, the damage initiations are multiple and the analysis could also require analysis of the crack population [**30, 43-44, 47**].
When some sites lead to the creation of cracks, the last key factor to consider is the resistance of the material to crack propagation as it will drive the ratio between the initiation and propagation durations during the lifetime and the fatigue scattering [**45, 48**]. This scale is maybe the one where the link between macroscopic and microscopic features seems clearer, throughout fracture mechanics [**21, 45**]. Nevertheless, the hypotheses required can be disputable, especially for filled materials and large strains [**25**], and the correlation between the so-called effective flaw features and the ones of the critical inclusions measured can be not straightforward [**25, 43**].

The aim of the study is to combine the evaluation of the dissipated energy, based on thermal measurements, with the evolution of the crack population, evaluated from interrupted fatigue tests using SEM measurements [**10, 11**], and to challenge the capacity of this approach to predict the fatigue curve. The focus is given here on a fully formulated Natural Rubber (NR) filled with carbon black because this material presents high industrial interest for fatigue applications and is a typical example of multi-initiation under cyclic loading.

A first section presents the material investigated and the sample geometry. In a second section, the experimental protocols used for the thermal characterization and the approach applied to determine the cyclic dissipated energy from the thermal measurements are presented. The curve relating the dissipated energy per cycle to the strain amplitude is called the heat build-up curve. The third section presents the experimental protocols used for the fatigue tests (both classic and interrupted) and the evolution of the defects population along the fatigue cycles, obtained from a wide programme of SEM observations. This investigation describes the population of cracks initiated at the skin of the fatigue samples and presenting a size over 5 micrometres. The results obtained are discussed and the dependencies of the cracks surface density on strain and fatigue cycles are described. In a last section, an energy based criterion is suggested, combining the evolution of the dissipated energy and the crack surface density. Finally, the predictions obtained with this criterion are compared with the Wöhler curve built from classic fatigue tests.

1. MATERIAL AND SAMPLES

The elastomer investigated in this study was an NR filled with CB and vulcanized with sulfur. The chemical composition is given in Table I.

Constituent	Amount [phr]
Natural Rubber (NR)	100
Carbon black (CB) type N550	43
Zinc oxyde	5
Sulfur	1.8
CBS	2.5
Stearic acid	2
Plasticizer	3
Anti-oxydants	2

TABLE I: Chemical composition of the compound investigated (so-called NR43)

The experiments were conducted on hourglass-shaped samples, designated AE2. Its geometry is given in Figure 1. This geometry was chosen for several reasons. First, it is classically used to obtain Wöhler curves. Then, the initiation and failure zone is controlled and located in the thinnest section. Moreover, the process is representative of that used for industrial parts. Finally, the thin section leads to limited self-heating for the frequencies considered here, even at the core of the sample, which prevents any coupled effects due to temperature rise during the fatigue tests.

Figure 1. AE2 sample geometry.

It should be underlined that, although this complex shape presents several interests [**10**], its main drawback is the complex mechanical fields induced by uniaxial tension. This drawback can also be an advantage, as explained in section 3 dealing with microstructural investigations. Moreover, it would, for example, be very difficult to provide an energy analysis based on the macroscopic hysteretic loop (i.e. force-displacement response). This is why the evaluation of the dissipated energy is based on the measurement of the thermal fields, as presented in the next section.

2. GENERATION OF THE HEAT BUILD-UP CURVE

2.1. THERMAL DEVICES

The thermal acquisition was performed thanks to a FLIR SC7600-BB infrared camera. The device is equipped with a Stirling-cycle cooled Indium-Antimonide (InSb) Focal Plane Array (FPA). The FPA is a 512*640 array of detectors digitized on 14 bits and sensitive in the 1.5-5.1µm spectral band whose pitch (distance between two detectors) is 15µm. The optical lens is designated “G1”, the focal distance is 300mm and the pixel size is 15µm. For all the experiments, the integration time was set to 1800µs.

In order to improve the thermal resolution (compared to classic thermal calibration), a homemade pixel-wise calibration (with an extra correction taking into account the influence of the internal camera temperature) was used. The details can be found in [**10**, **49**].

After this specific calibration, precision of about 10mK is obtained for differential measurements.

2.2. HEAT BUILD-UP PROTOCOL

All mechanical tests used to generate the heat build-up curves were achieved on a Bose ElectroForce 3330 testing instrument. The 3330 system provides static to 100 Hz performance with a load capacity of ±3200N and a displacement range of ±12.7mm. All the experiments were displacement controlled. Special attention was paid to the experimental conditions in order to avoid as much as possible the influence of the environment on the measurements. The sample was surrounded by a black card box to limit any reflections and a dark sheet covered the experimental set-up (Figure 2).

Figure 2. Experimental set-up for thermal measurements.

The principle of a heat build-up protocol basically consists of submitting a sample to a succession of cyclic tests of increasing displacement amplitude (Figure 3), and to record for each sequence the evolution of the temperature. Thirteen blocks were performed for several displacement amplitudes between 1mm and 13mm (corresponding to a maximal principal strain at skin of 15% and 250% respectively at the central section of the AE2).

Figure 3. Heat build-up protocol.

The analysis of the dissipated energy from the thermal resolution requires solving the heat equation, as presented in section 3. This analysis can be based either on a stationary state or on an adiabatic hypothesis lead over the first cycles [**17, 50-51**]. The choice of the mechanical protocol depends of course on the chosen analysis. In this study, adiabatic analysis was selected, which leads to a mechanical protocol focused on the first loading cycles.

Each loading block was composed of three stages (see figure 3). In order to limit the influence of the Mullins effect and to reach a stabilized cyclic response, representative of the fatigue cycles, a first stage consisted in submitting the sample to 10 cycles to accommodate the response for the displacement amplitude considered in this block. The mechanical frequency was 2Hz, similar to that used for the fatigue tests. Parts used for automotive applications could of course undergo higher frequencies but the idea here is to be representative of the fatigue tests conditions. Moreover, some other studies showed that the evaluation of the dissipated energy was not dependant on the frequency [51] .The second stage was a cooling step lasting 200s, in order to let the sample cool to the ambient temperature and to have comparable initial conditions from one loading block to another. As the rise of temperature is very low during the loading step, no thermal stresses are likely to occur during this cooling stage under constant displacement. The third stage was the loading step, for which the sample was submitted to displacement controlled cyclic loading of 30 cycles at the amplitude considered in the block. The mechanical frequency was also 2Hz. During this stage, thermal acquisition was performed, supplying the thermal images that will be analysed to follow the temperature evolution and to determine the dissipated energy (see [**17**] for more details).

This mechanical protocol was repeated for each block, and allowed relating the dissipated energy to the displacement amplitude.
The last block ran until failure of the sample occurs, giving extra fatigue data for high strains.

2.3. THERMAL MEASUREMENTS AND DETERMINATION OF THE CYCLIC DISSIPATED ENERGY

Thermal acquisition was performed using a rate of 30 images per second in order to provide 15 images per cycle, which leads to a good description of the mechanical configuration of the sample. The thermal acquisitions were done on the sample at the maximal deformed position (Figure 4a) because this provides the best controlled geometrical configuration. Figure 4a illustrates the thermal fields of the sample under extension. For each loading block, the temperature was averaged over the black rectangle visible on Figure 4a.

Figure 4. Typical thermal measurements during one block of the heat build-up protocol.

Figure 4b presents the typical evolution of this mean temperature. A rise of the mean temperature is observable. The temperature oscillations visible on the curve are not directly related to the thermo-elastic couplings as the computation zone is fixed while the material points are moving during the experiment. This is why in the following parts of the paper only the temperature fields evaluated for the same spatial configuration are considered (marked with crosses on Figure 4b).

To determine the cyclic dissipated energy from thermal measurements, an experimental approach has been developed and validated in recent papers [**30, 47, and 51**]. The basic idea is to use an adiabatic hypothesis to estimate the dissipated energy from the first cycles. It is worth underlining that the temperature rise is very limited within the 30 cycles imposed, whatever the displacement amplitude imposed, and that the temperature stabilization, due to exchange by conduction and convection, is not reached. The specific details are presented in [**17**] and will not be recalled here.

As explained in section 2, several blocks of loading with increasing displacement amplitudes were performed. For each loading block, the dissipated energy was evaluated on the central area of the sample. It is, therefore, possible to plot a heat build-up curve, relating this energy to the local maximum principal strain.

The heat build-up curve is presented on Figure 5. A polynomial fit gives a good evaluation of the dependency of the dissipated energy par cycle, termed Δ^*, to the local maximum principal strain ε. This analytical fit will be used in section 4 to feed the fatigue criterion.

Figure 5. Heat build-up curve relating the dissipated energy per cycle to the local maximum principal strain.

3. EVALUATION OF THE FATIGUE CRACKS POPULATION

3.1. INTERRUPTED FATIGUE TESTS

The classic fatigue tests were performed with AE2 samples by Vibracoustic (see Figure 1). The fatigue tests were monitored with prescribed displacement and for a minimum displacement equal to 0 mm. No mechanical conditioning was performed on samples before fatigue tests. The full Wöhler curve was built on 5 displacement levels with 5 samples for each level. The experimental determination of the fatigue initiation was achieved using an end-of-life criterion based on the variation of the effective stiffness [**52**]. The variation of

effective stiffness was identified as a first regime related to the relaxation of visco-elasticity (decrease following a semi-logarithmic relation) and a deviation from this slope related to fatigue damage. The criterion is detailed elsewhere [51] and corresponds to the initiation of a 2 mm crack.
Based on this first evaluation, an experimental programme was defined in order to generate samples cycled for 20, 40% and 60% of the average fatigue lifetime, for three imposed displacements leading to three maximum local strains (60, 100%, 200%). Nine samples were, therefore, generated this way. The principle of these interrupted fatigue tests is illustrated in Figure 6. The validity of this approach is supported by the very low scattering of the fatigue lifetime results obtained on the considered material.

Figure 6. Illustration of the interrupted fatigue tests.

3.2. SEM OBSERVATIONS

The SEM investigations were performed with a JEOL 6060-LA and the images were taken by using the secondary electrons signal. The details of the observation parameters can be found elsewhere [**10, 11**]. The nine samples generated thanks to the interrupted fatigue campaign were characterized. The sample was slightly stretched (3 mm of global extension) in order to ease detection of the initiated cracks. For each sample, an area centered on the minimal section was observed.
This area was divided into 5 slices with a height of 0.75mm (see Figure 7). To observe the whole circumference of the samples, this operation was repeated four times, after successive rotations of 90°.

Figure 7. Field of the maximum strain field and illustration of the areas investigated for the SEM measurements

For the considered experimental conditions and compound, the fatigue initiation always appeared at multiple locations, at the parting line or out of the parting line. For each slice, only cracks longer than 5 µm are considered here, whatever the nature of the inclusion or the geometric defect giving birth to this crack [**10, 11**]. The number of cracks observed for each slice was divided by the surface of the slice in order to evaluate a crack surface density. This value can then be related to the strain at the skin of the slice considered. The values of slices 2 and 2’ (3 and 3’ respectively) were averaged in order to improve the statistical evaluation. Finally, this means that each tested sample provided 3 crack surface densities, related to 3 maximum local strains. It is worth underlining here that this evaluation of the defect population over a surface gives a reliable evaluation of the overall defect population as the cracks are initiated mainly at the skin in the case of this sample geometry and for this well dispersed compound [**10, 11, and 30**].

3.3. RESULTS

Figure 8 illustrates the evolution of the cracks surface density along the fatigue cycles for the three tested samples. For each sample, the crack surface density was evaluated over the 5 slices, as explained before, and, therefore, gives access to the evolution for three local strains experienced on the skin. For each strain, the three points correspond respectively to 20%, 40% and 60% of the average fatigue life (initiation criterion) of the sample. This fatigue life is also recalled on the graph by the dotted lines. These values are those obtained from the classic fatigue tests for maximum local strain of 200%, 101% and 60% respectively.

Figure 8. Evolution of the cracks surface density with the fatigue cycles.

These curves provide a few interesting results. First, cracks initiation starts early in the fatigue life (before 20% of the fatigue life) and grows quite slowly with fatigue cycles, except for the highest strain. Second, the evolution rates of the crack surface density are ranked in a consistent way with the local maximum strain. Third, it seems that the fatigue life is not determined by a critical value of crack surface density as the values reached for the three samples are different. These observations illustrate fatigue behavior mostly driven by early initiation and subsequent crack propagation, which seems well correlated to the very low scattering obtained for fatigue life (Figure 6). Let us recall here that the fatigue criterion used here is an initiation criterion, based on the stiffness evolution and leading to a maximum crack length of 1 mm.

4. PREDICTION OF THE WOHLER CURVE BASED ON A ENERGETIC CRITERION USING A SINGLE PARAMETER

4.1. PROPOSAL OF AN ENERGETIC CRITERION BASED ON THE EVOLUTION OF THE CRACKS DENSITY AND ON THE DISSIPATED ENERGY

Now that the local strain is related to the dissipated energy, the idea is to use an energy based criterion to relate the dissipated energy to the fatigue lifetime. To build this relation, it is first of all very important to be sure that the evaluation of the dissipated energy is done over the appropriate volume, i.e. the volume in which the fatigue initiation occurs. For the materials considered here, a thorough study using SEM and X-ray measurements [**10, 11, 30**] demonstrated that the failure occurs at the skin of the samples, in the central area of the diabolo-shaped specimens. The protocol chosen in this study to evaluate the dissipated energy is based on an almost adiabatic analysis. This means that the dissipated energy measured is related to a small amount of the material in the vicinity of the surface, as the conduction within the depth is very limited, due to the short duration considered. A numerical study of the depth over which the dissipated energy is measured was achieved [**10**] and showed that this distance is around 0.8 mm. Therefore, the evaluation of the dissipated energy seems fully consistent with the location of the fatigue initiation, and a relation between the dissipated energy evaluated and the fatigue lifetime can be investigated.

In former studies [**10, 17, 47**], a protocol using thermal measurements to predict the fatigue life throughout an energy based criterion proved to afford a very efficient prediction of the deterministic Wöhler curve (one sample, within less than one day) and for various compounds. This very efficient approach is based on thermal data only and uses a fatigue criterion relating the number of cycles to initiation to the cyclic dissipated energy Δ^* with two parameters b and E that need to be identified:

$$\Delta^* N^b = E \qquad (1)$$

In the present study, the objective is different, as the focus is not on the fast aspect of the determination since the microstructural investigations take time. The goal is to avoid any assumption of the mathematical shape of the energetic function and to feed the basic equation of the dissipation based criterion with the data provided by microstructural observations and thermal measurements.

The basic idea is first to consider that, for each cycle, the material dissipates some energy $E_{diss,f}$ related to fatigue mechanisms, and possibly dependent on the local strain and on the cycle considered. The material is then assumed to fail when a critical value E_D of this energy is accumulated:

$$E_D = \int_0^{Ni} E_{diss,f}(\varepsilon, N)dN \qquad (2)$$

To evaluate the energy related to the fatigue mechanisms $E_{diss,f}$, a first way would be to compute and sum the dissipated energy for every fatigue damage site (inclusions, geometric defect, cracks). This could be possible as the fatigue damage sites activated are identified by the microstructural observations but, beyond the computation times required, for a given fatigue damage site, the thermomechanical characterization is still missing to feed and validate the models. In this study, the scale of the defects population is considered instead, and the energy related to fatigue mechanisms $E_{diss,f}$ is assumed to be a fraction of the total dissipated energy per cycle Δ* with a ratio proportional to the cracks density $\varpi d(\varepsilon, N)$:

$$E_{diss,f}(\varepsilon, N) = \Delta^*(\varepsilon).\, \varpi d(\varepsilon, N) \qquad (3)$$

The next step of the approach is to determine the evolutions of Δ*(ε) and $\varpi d(\varepsilon, N)$. The evolution of the dissipation is not dependent on the fatigue cycles and can be extracted from the integral, and then comes easily from the heat build-up curve. On the contrary, the crack surface density evolves both with strain and fatigue cycles, and an analytical law needs to be identified to go further.

4.2. DESCRIPTION OF THE EVOLUTION OF THE CRACKS DENSITY ALONG THE FATIGUE LIFETIME

The description of the defects population was evaluated thanks to the SEM measurements achieved on samples submitted to interrupted fatigue tests (see Section 3). It is worth noting that $\varpi d\ (\varepsilon, N)$ is, in this case, a surface density as the fatigue initiation occurs exclusively on this area, although the approach suggested above could of course be defined for a crack volume density.

Figure 9 illustrates the evolution of this crack density along the fatigue cycles for several maximum principal strains. This curve presents the same results as in Figure 8, but using a linear scale for the axis of the fatigue cycles. One can see that the strain is a first order parameter driving the evolution of the crack surface density. In order to provide a common description for all the strains investigated, a linear evolution with the number of cycles can be suggested as an approximation, as illustrated on Figure 9. The slope of this linear evolution $K(\varepsilon)$ depends strongly on the strain and reasonably follows a power law, as illustrated on Figure 10.

Following this approach, $\varpi d(\varepsilon, N)$ can be expressed as:

$$\varpi d(\varepsilon, N) = K(\varepsilon).N \qquad (4)$$

It is worth noting that this description of the fatigue cracks is not related to a given percentage of fatigue life but only to the number of cycles experienced.

Figure 9. Evaluation of the kinetic of the cracks surface density along the fatigue cycles.

Figure 10. Determination of the relation between the slope of the kinetic of creation of surface cracks and the local strain.

4.3. CHALLENGE OF THE CRITERION

The last step of the approach is now to replace the evolutions $\Delta^*(\varepsilon)$ and $\varpi d(\varepsilon, N)$ and to relate the dissipated energy to the strain ε and the fatigue life N_i.

Replacing $\varpi d(\varepsilon, N)$ in Equation 3 and using Equation 2, results in:

$$E_D = \Delta^*(\varepsilon).K(\varepsilon)\int_0^{Ni} N.dN \qquad (5)$$

and the energy criterion finally written as:

$$E_D = \Delta^*(\varepsilon).K(\varepsilon).\frac{Ni^2}{2} \qquad (6)$$

It is important to underline that E_D is the only parameter to be identified, as $\varpi d(\varepsilon, N)$ and $\Delta^*(\varepsilon)$ are measured from experiments.

A first way to challenge this criterion is to check if the values of E_D computed for several maximum local strains are comparable.

Table 2 shows the results obtained for various values of local maximum strain. The fatigue life was obtained from the classic fatigue test, the slope $K(\varepsilon)$ was evaluated from the power law given on Figure 10 and $\Delta^*(\varepsilon)$ was evaluated from the polynomial fit of the heat build-up curve given in Figure 5. Even if the value obtained for the 60% is a little bit lower, the critical dissipated energy appears very close to a constant and could be considered as an intrinsic parameter of the material.

Maximum local strain ε	Fatigue cycles to initiation N_i	Rate of defects creation $K(\varepsilon)$	Dissipated energy par cycle $\Delta^*(\varepsilon)$	Critical dissipated energy E_D
60	85000	$1{,}92.10^{-5}$	21,7	$1.51.10^{8}$
100	183180	$2.4.10^{-4}$	57,4	$2.32.10^{8}$
130	70000	$8{,}8.10^{-4}$	95.3	$2.06.10^{8}$
170	30000	$3.3.10^{-3}$	160.7	$2.41.10^{8}$
200	17759	$7.4.10^{-3}$	220.8	$2.59.10^{8}$

TABLE II: Evaluation of the Critical Cumulated Energy ED.

Another, more elegant way to check the validity of the criterion is to use the value of E_D obtained for a given strain and to plot the full predicted fatigue curve, using the analytical functions identified for $K(\varepsilon)$ and $\Delta^*(\varepsilon)$ (see Figures 5 and 10). Here, E_D is taken as the mean value of those presented in the Table II.

Figure 11 compares the predicted fatigue curve to the experimental values. Very good agreement is indeed observed for the full fatigue curve.

Figure 11. Fatigue curve predicted and experimental values.

CONCLUSIONS

The goal of this paper was to relate the fatigue lifetime to the dissipation and the defects population for a Natural Rubber (NR) compound filled with carbon black. In a first section, the building of the heat build-up curve was presented, relating the dissipated energy at skin to the local maximum principal strain.

Then, the evolution of the defect population was investigated thanks to interrupted fatigue tests and SEM observations. The conclusions of this work are: (1) the cracks initiate early in the fatigue life (before 20% of the fatigue life) and grows quite slowly with the fatigue cycles, except for the highest strains; (2) the kinetics of the crack surface density are ranked in a consistent way with the local maximum strain; (3) the fatigue life seems not determined by a critical value of crack surface density. These observations illustrate fatigue behaviour mostly driven by an early initiation and subsequent crack propagation, which seems well correlated to the very low scattering obtained for fatigue lives.

Finally, a fatigue criterion is suggested, starting from the basic assumption of accumulation of dissipated energy along the fatigue cycles. The ratio between the global energy dissipated and the energy related to the fatigue mechanisms is assumed to be driven by the crack surface density. The dissipated energy is evaluated from the thermal measurements and the evolution of the crack surface density with strain and fatigue cycles is described. Combining these two functions, the energetic criterion can be written as a simple expression using a single parameter. The predictions obtained with the criterion identified were compared with the results from classic fatigue tests and very close agreement was found.

Compared to recent studies based only on thermal measurements [**10, 17, 47**], the evaluation of the fatigue properties is not fast anymore as the microstructural analysis requires some time, but the very good agreement between the predicted fatigue curve and the mean experimental curve supports the physical meaning of an approach based on dissipated energy.

ACKNOWLEDGEMENTS

The authors would like to thank the ANR for its financial support (ANR–2010–RMNP-010-01) and all the partners of the PROFEM project, Vibracoustic, IRDL, GeM, UBS and LRCCP. A special thanks to S. Noizet, C. Schiel and O. Brozkewicz for their careful SEM investigations.

REFERENCES

1. A. A. Griffith, Phil. Trans. R. Soc. London A Math. Phys. Eng. Sci. 221, 582 (1921).

2. J. R. Beatty, RUBBER CHEM. TECHNOL. 37, 1341 (1964).
3. A. N. Gent, P. B. Lindley, and A. G. Thomas, J. Appl. Polym. Sci. 8, 455 (1964).
4. Gent, A. N. & B. Park 1984. Failure processes in elastomers at or near a rigid spherical inclusion. Journal of Materials Science, 19, 1947-1956.
5. S.V. Hainsworth. An environmental scanning electron microscopy investigation of fatigue crack initiation and propagation in elastomers. Polym. Test., 26 (2007), pp. 60–70.
6. Choi IS, Roland CM. Intrinsic defects and the failure properties of cis-1,4-polyisoprenes. Rubber Chemistry and Technology. 1996;69:591–9.
7. Beurrot, S., B. Huneau & E. Verron 2010. In situ SEM study of fatigue crack growth mechanism in carbon black-filled natural rubber. Journal of Applied Polymer Science, 117, 1260-1269.
8. JB Le Cam, B Huneau, E Verron. Fatigue damage in carbon black filled natural rubber under uni-and multiaxial loading conditions, International Journal of Fatigue, 52, 82-94, 2013.
9. V. Le Saux. “Fatigue et vieillissement des élastomères en environnements marin et thermique: de la caractérisation accélérée au calcul de structure”, V. Le Saux, Ph.D. thesis, 2010.
10. I. Masquelier. PhD thesis, Université de Bretagne Occidentale, 2014.
11. B. Huneau, I. Masquelier, Y. Marco V. Le Saux, S. Noizet, C. Schiel, P. Charrier, Fatigue crack initiation in a carbon black-filled natural rubber. Rubber Chemistry and Technology, 89 (1), 126-141, 2016.
12. Mars W. & Fatemi A., 2002. A literature survey on fatigue analysis approaches for rubber. International Journal of Fatigue, 24, 949-961.
13. M. Cadwell, R. Merril, C. Sloman, F. Yost. Dynamic fatigue life of rubber. Indus Eng Chem, 12 (1) (1940), pp. 19–23.
14. Roberts, B.J., Benzies, J.B., 1977. The relationship between uniaxial and equibiaxial fatigue in gum and carbon black filled vulcanizates. in: Proceedings of Rubbercon’77, vol. 2.1, pp. 1–13.
15. F. Abraham, T. Alshuth, S. Jerrams. The effect of minimum stress and stress amplitude on the fatigue life of non-strain crystallising elastomers. Mater. Design, 26 (2005), pp. 239–245.
16. N. André, G. Cailletaud, R. Piques. Haigh diagram for fatigue crack initiation prediction of natural rubber components. Kautsch Gummi Kunstst, 52 (1999), pp. 120–123
17. Y. Marco, I. Masquelier, V. Le Saux and P. Charrier. Fast prediction of the Wöhler curve from thermal measurements for a wide range of NR and SBR compounds. Rubber Chemistry and technology. In press, 2016.
18. A.N. Gent, P.B. Lindley, A.G. Thomas. Cut growth and fatigue of rubbers. I. The relationship between cut growth and fatigue. J. Appl. Polym. Sci., 8 (1964), pp. 455–466.
19. R. Rivlin, A. Thomas. Rupture of rubber part 1: characteristic energy for tearing. J Polym Sci, 10 (1953), pp. 291–318.
20. P. Lindley. Energy for crack growth in model rubber components. J. Strain Anal., 7 (1972), pp. 132–140
21. Gent, A. N., and W. V. Mars. "Strength of Elastomers, the Science and Technology of Rubber. Chapter 10." (2013).
22. W. Mars. Cracking energy density as a predicting factor of fatigue life under multiaxial conditions. Rubber Chem Technol, 75 (2002), pp. 1–15
23. N. Saintier, G. Cailletaud, R. Piques. Crack initiation and propagation under multiaxial fatigue in a natural rubber. International Journal of Fatigue, Volume 28, Issue 1, January 2006, Pages 61–72
24. E. Verron, A. Andriyana. Definition of a new predictor for multiaxial fatigue crack nucleation in rubber. Journal of the Mechanics and Physics of Solids. Volume 56, Issue 2, February 2008, Pages 417–443
25. J. G. R. Kingston and A. H. Muhr. Determination of effective flaw size for fatigue life prediction. Constitutive Models for Rubber VII. CRC Press. pp. 337–342. 2011.
26. Le Gorju Jago, K. 2012. X-ray computed microtomography of rubber. Rubber Chemistry and Technology, 85, 387-407.
27. Le Saux, V., Y. Marco, S. Calloch & P. Charrier 2011. Evaluation of the fatigue defect population in an elastomer using X-Ray Computed micro-tomography. Polymer Engineering and Science, 51, 1253-1263.

28. K. Legorgu-jago and C. Bathias, Int. J. Fatigue, 24, 85, 2002.
29. K. Le Gorgu Jago, Constitutive Model for Rubber V, Paris, France, 173 (2007).
30. Y. Marco, I. Masquelier, V. Le Saux, S. Calloch, B. Huneau, P. Charrier, Contributions of IR thermography and X-ray tomography to the fatigue characterization of elastomeric materials, The 8th European Conference on Constitutive Models for Rubbers (ECCMR VIII)**,** San Sebastian, **2013.**
31. N. Saintier, G. Cailletaud, and R. Piques, Int. J. Fatigue 28, 61 (2006).
32. H. Dal, M. Kaliske . A micro-continuum-mechanical material model for failure of rubberlike materials: Application to ageing-induced fracturing. J. Mech. Phys. Solids 57 (2009) 1340–1356.
33. Saintier N. Multiaxial fatigue life of a natural rubber: crack initiation mechanisms and local fatigue life criterion. PhD Dissertation, Ecole des Mines de Paris.
34. Y. Fukahori and W. Seki, *J. Mater. Sci.*, 28, 4471 (1993).
35. I. Masquelier, Y. Marco, V. Le Saux, B. Huneau, F. Rouillard, P. Charrier, Thermomechanical characterization of the basic fatigue mechanisms at the inclusions' scale. The 9th European Conference on Constitutive Models for Rubbers (ECCMR IX), Prague. 2015.
36. Lion, A., 1996. A constitutive model for carbon black filled rubber: experimental investigations and mathematical representation. Continuum Mech. Thermodyn. 8, 153–169.
37. Bergström, J.S., Boyce, M.C., 2000. Large strain time-dependent behavior of filled elastomers. Mech. Mater. 32, 627–644.
38. Miehe, C., Keck, J., 2000. Superimposed finite elastic–viscoelastic–plastoelastic stress response with damage in filled rubbery polymers. Experiments, modeling and algorithmic implementation. J. Mech. Phys. Solids 48, 323–365.
39. Laiarinandrasana, L., Piques, R., Robisson, A., 2003. Visco-hyperelastic model with internal state variable coupled with discontinuous damage concept under total Lagrangian formulation. Int. J. Plasticity 19, 977– 1000.
40. N. Candau, L. Chazeau, J-M. Chenal, C. Gauthier, J. Ferreira, E. Munch, D. Thiaudière. Strain induced crystallization and melting of natural rubber during dynamic cycles. Physical Chemistry Chemical Physics. May 2015
41. B Huneau. Strain-induced crystallization of natural rubber: a review of x-ray diffraction investigations. Rubber chemistry and technology 84 (3), 425-452. 2011.
42. Julie Diani, Bruno Fayolle, Pierre Gilormini. A review on the Mullins effect. European Polymer Journal, Elsevier, 2009, pp.601-612.
43. F. Abraham. Definition and use of an effective flaw size for the simulation of elastomer fatigue. In: Jerrams, S. and Murphy, N., eds. Constitutive models for rubber VII:. CRC Press Inc, London, pp. 331-335. 2012.
44. S. Rausch, M. A. Ruderer, W. Enke, A. Narváez, M. Ludwig, T. Alshuth. Lifetime prediction of elastomer components within gasoline engines. Constitutive Models for Rubbers IX. Pages 363–366. 2015.
45. W. V. Mars (*2007*) Fatigue Life Prediction for Elastomeric Structures. Rubber Chemistry and Technology: July 2007, Vol. 80, No. 3, pp. 481-503.
46. R. J. Harbour, A. Fatemi, W. V. Mars. Fatigue life analysis and predictions for NR and SBR under variable amplitude and multiaxial loading conditions. International Journal of Fatigue 30, 1231–1247, 2008.
47. V. Le Saux, Y. Marco, S. Calloch, C. Doudard, P. Charrier, Fast evaluation of the fatigue lifetime of elastomers based on a heat build-up protocol and micro-tomography measurements, International Journal of Fatigue, 32 (10), pp. 1582-1590, 2010.
48. M. Ludwig, T. Alshuth, M. El Yaagoubi, D. Juhre . Lifetime prediction of elastomers based on statistical occurrence of material defects. Constitutive Models for Rubbers IX. Pages 445–448. 2015.
49. V. Le Saux and C. Doudard. Proposition of a compensated pixelwise calibration for photonic infrared cameras and comparison to classic calibration procedures: case of thermoelastic stress analysis. Infrared Physics and Technology, 80: 83-92, 2017.

50. G. La Rosa and A. Risitano. Thermographic methodology for rapid determination of the fatigue limit of materials and mechanical components. International Journal of Fatigue, 22(1) : 65–73, 2000.
51. I. Masquelier, Y. Marco, V. Le Saux, S. Calloch, P. Charrier. Determination of dissipated energy fields from temperature mappings on a rubber-like structural sample: Experiments and comparison to numerical simulations. Mechanics of Materials, Volume 80, Part A, January 2015, Pages 113-123
52. E. Ostoja Kuczynski, P. Charrier, E. Verron, L. Gornet, G. Marckmann. Crack initiation in filled natural rubber: experimental database and macroscopic observations. Constitutive Model for Rubber III, pages 3–10, London (UK), September 15-17th 2003.

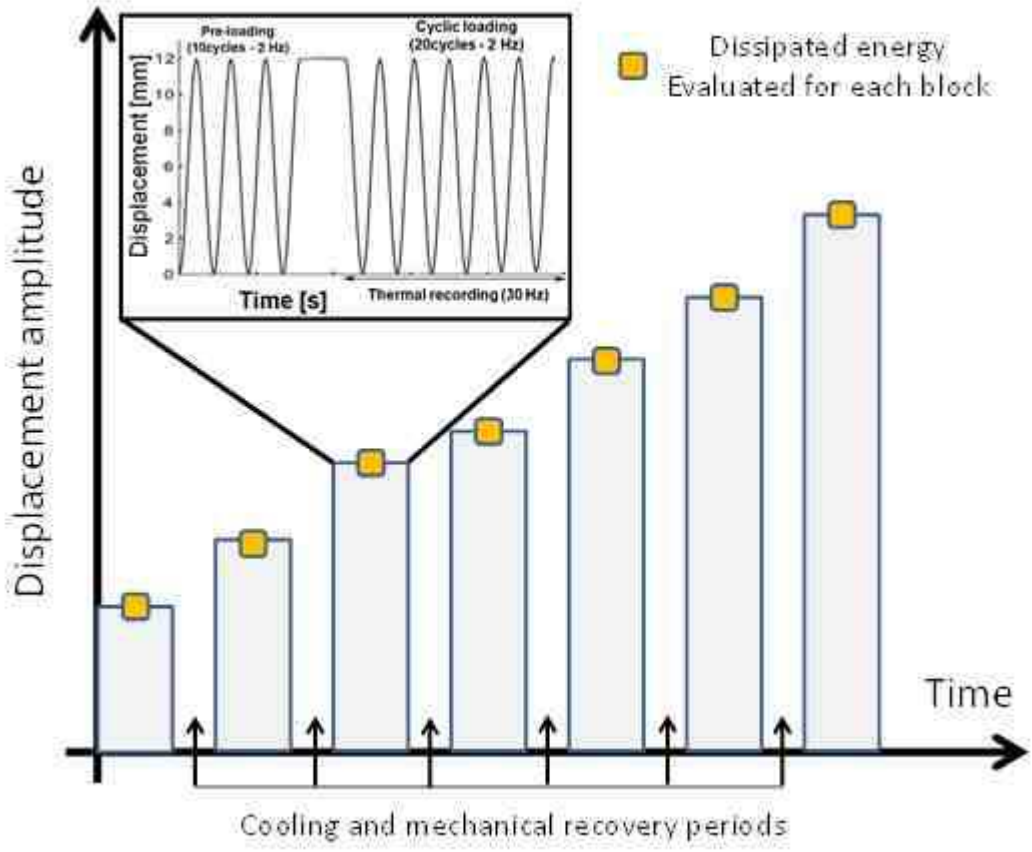
Pre-loading
(10cycles - 2 Hz)
Cyclic loading
(20cycles - 2 Hz)
Displacement [mm]
Time [s]
Thermal recording (30 Hz)
Dissipated energy
Evaluated for each block
Displacement amplitude
Time
Cooling and mechanical recovery periods

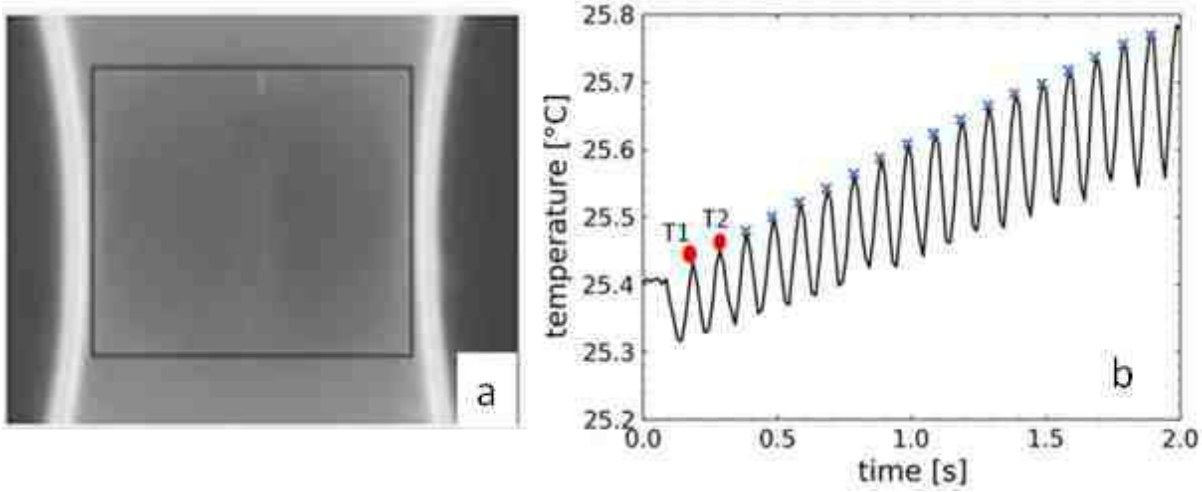
a
b
T1
T2
temperature [°C]
time [s]
25.8
25.7
25.6
25.5
25.4
25.3
25.2
0.0
0.5
1.0
1.5
2.0

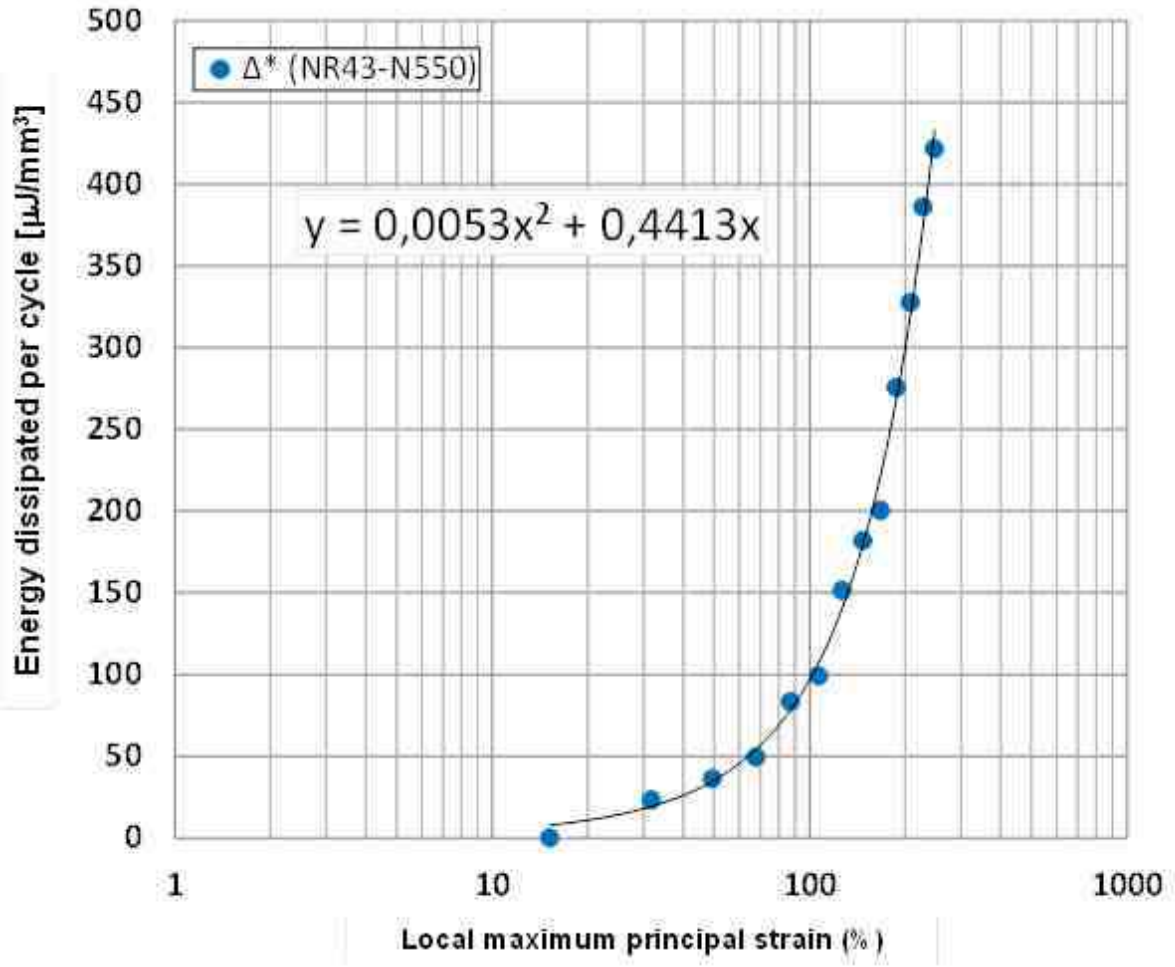
Δ* (NR43-N550)
y = 0,0053x² + 0,4413x
Energy dissipated per cycle [µJ/mm³]
Local maximum principal strain (%)
500
450
400
350
300
250
200
150
100
50
0
1
10
100
1000

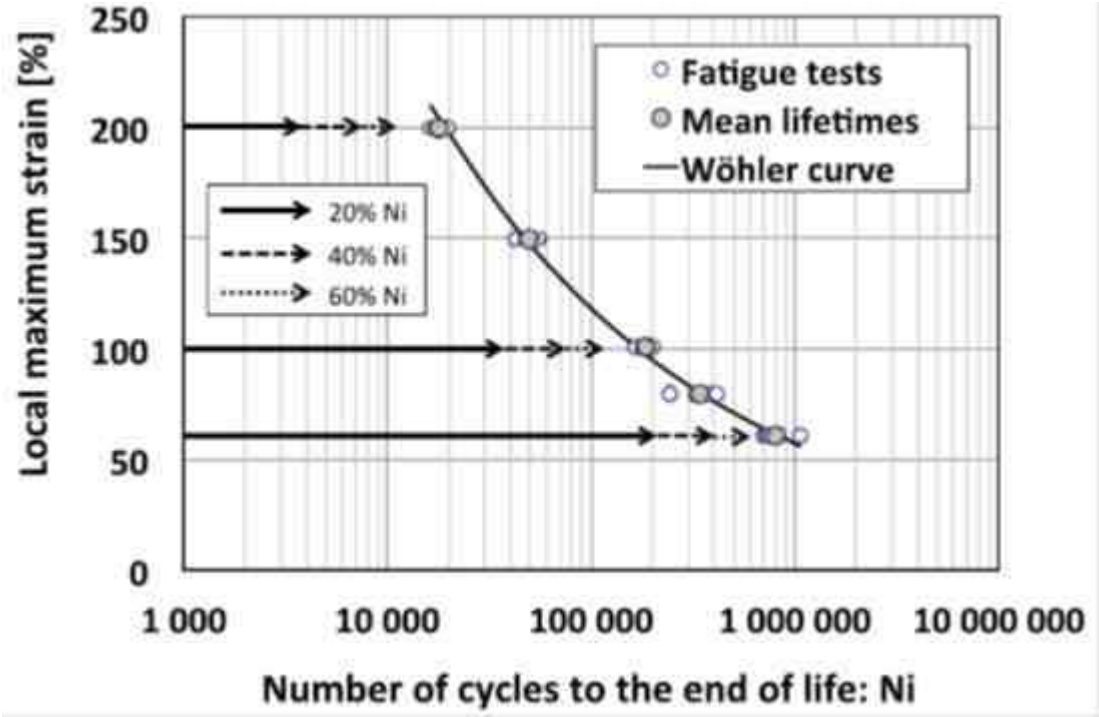
Local maximum strain [%]
250
200
150
100
50
0
1 000
10 000
100 000
1 000 000
10 000 000
Number of cycles to the end of life: Ni
Fatigue tests
Mean lifetimes
Wöhler curve
20% Ni
40% Ni
60% Ni

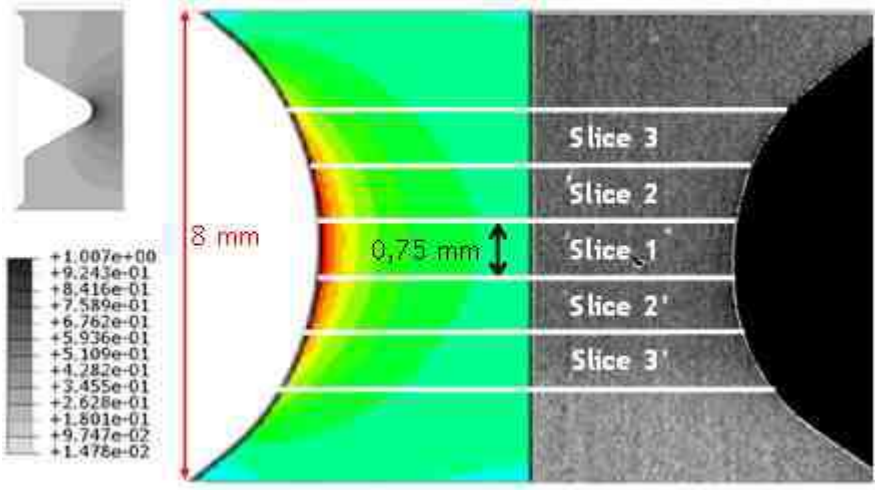
+1.007e+00
+9.243e-01
+8.416e-01
+7.589e-01
+6.762e-01
+5.936e-01
+5.109e-01
+4.282e-01
+3.455e-01
+2.628e-01
+1.801e-01
+9.747e-02
+1.478e-02
8 mm
0,75 mm
Slice 3
Slice 2
Slice 1
Slice 2'
Slice 3'

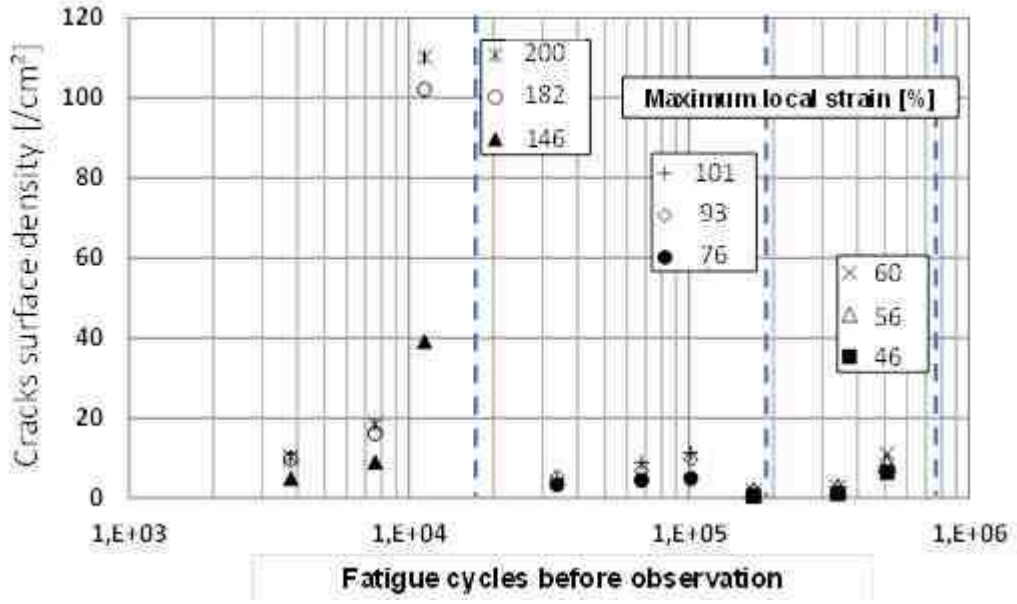
Cracks surface density [/cm²]
120
100
80
60
40
20
0
1,E+03
1,E+04
1,E+05
1,E+06
Fatigue cycles before observation
Maximum local strain [%]
200
182
146
101
93
76
60
56
46

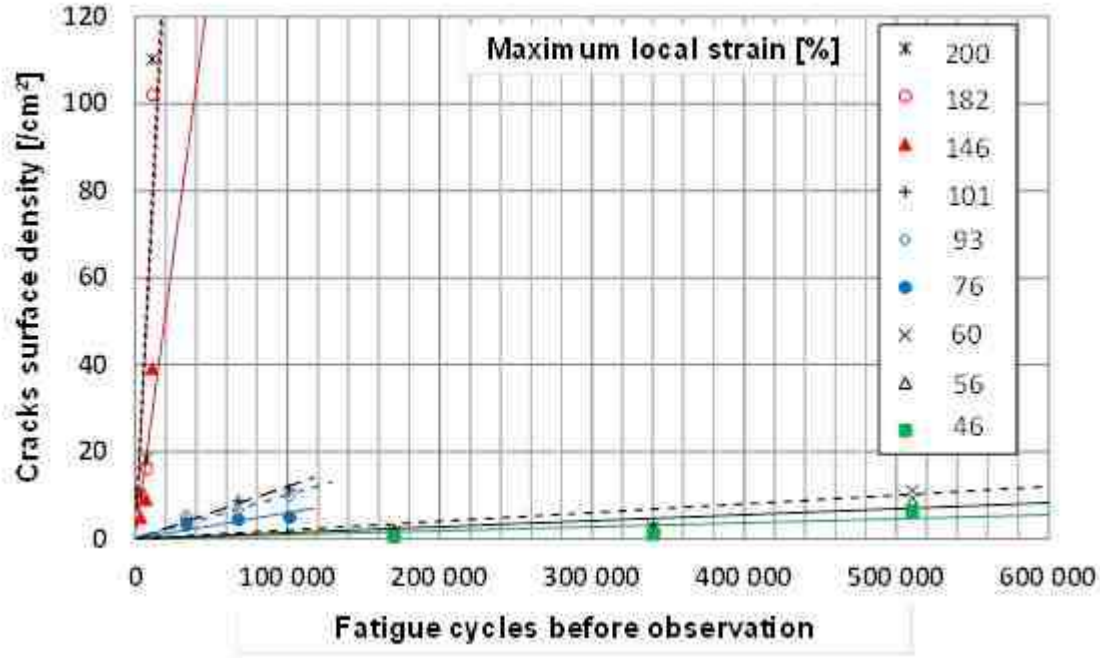
Maximum local strain [%]
200
182
146
101
93
76
60
56
46
Cracks surface density [/cm²]
120
100
80
60
40
20
0
0
100 000
200 000
300 000
400 000
500 000
600 000
Fatigue cycles before observation

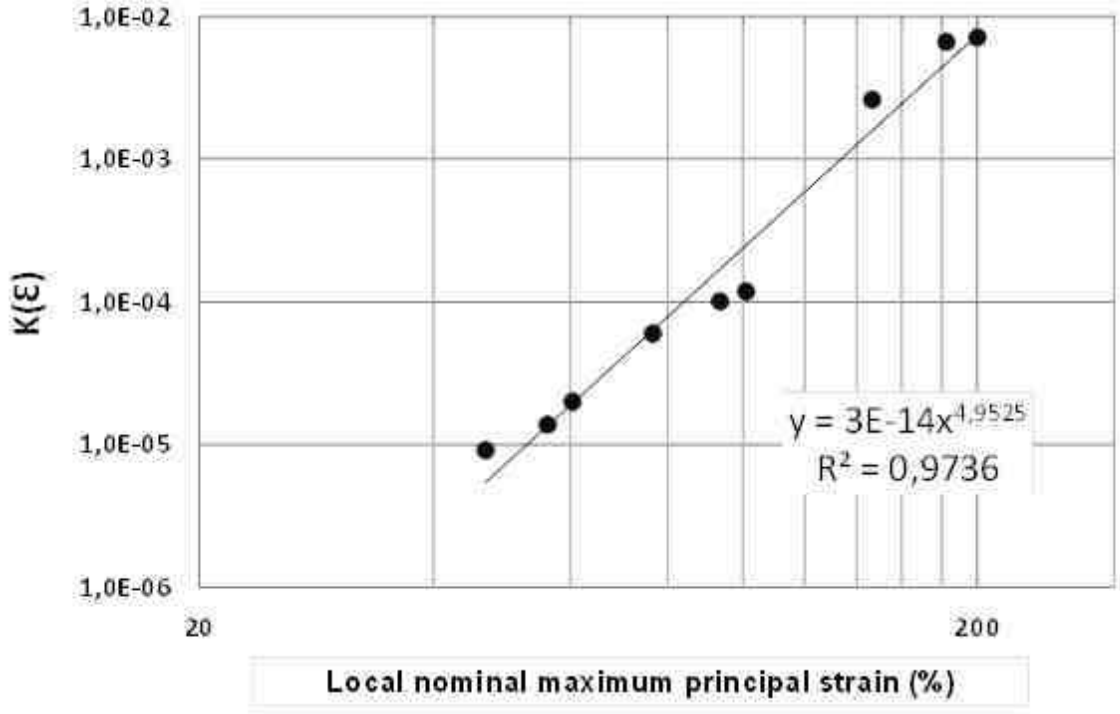
1,0E-02
1,0E-03
1,0E-04
1,0E-05
1,0E-06
K(ε)
20
200
y = 3E-14x^4,9525
R² = 0,9736
Local nominal maximum principal strain (%)

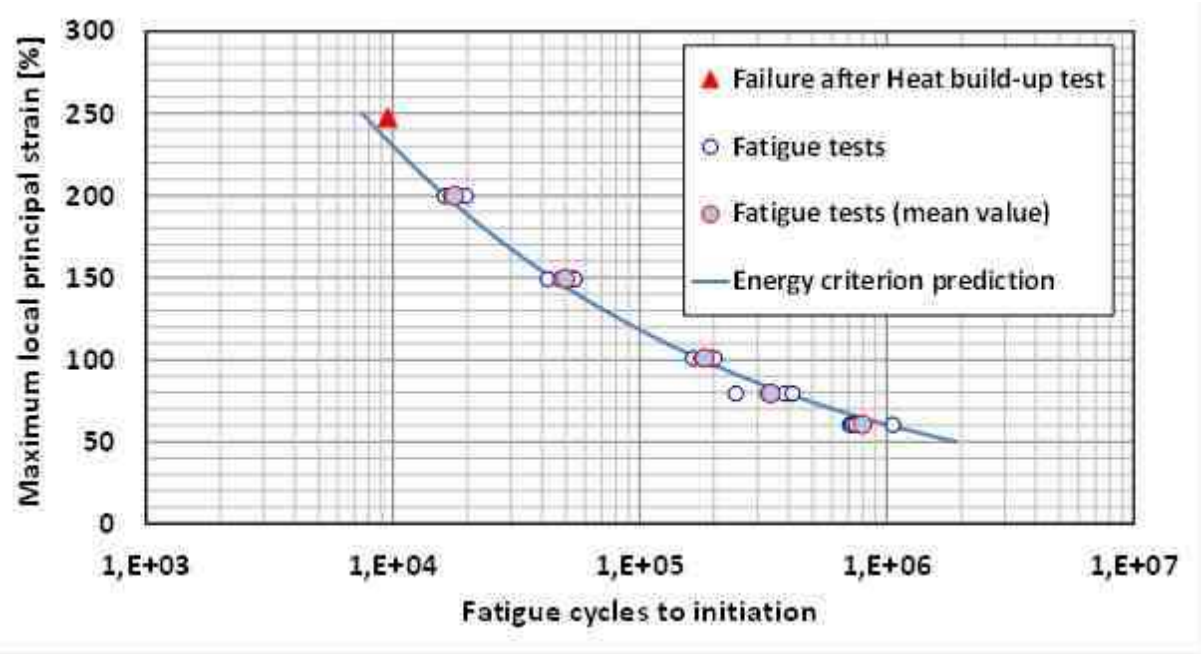
Maximum local principal strain [%]
300
250
200
150
100
50
0
1,E+03
1,E+04
1,E+05
1,E+06
1,E+07
Fatigue cycles to initiation
Failure after Heat build-up test
Fatigue tests
Fatigue tests (mean value)
Energy criterion prediction

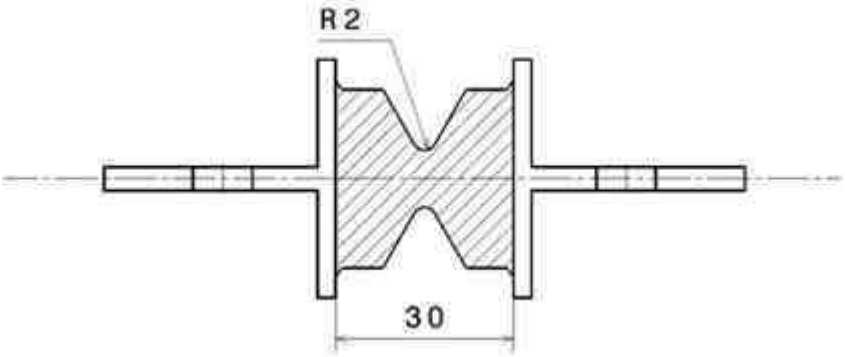
R2
30